

Performance analysis of lightweight CNN models to segment infectious lung tissues of COVID-19 cases from Tomographic images

Tharun J Iyer¹, Alex Noel Joseph Raj², Sushil Ghildiyal¹, Ruban Nersisson^{Corresp. 1}

¹ School of Electrical Engineering, Vellore Institute of Technology University, Vellore, Tamil Nadu, India

² Department of Electronic Engineering, Shantou University (汕头大学), Shantou, Guangdong, China

Corresponding Author: Ruban Nersisson
Email address: nruban@vit.ac.in

The pandemic of Coronavirus Disease-19 (COVID-19) has spread around the world causing an existential health crisis. Automated detection of COVID-19 infections in the lungs from Computed Tomography (CT) images offers huge potential in tackling the problem of slow detection and augments the conventional diagnostic procedures. However, segmenting COVID-19 from CT Scans is problematic, due to high variations in the types of infections and low contrast between healthy and infected tissues. While segmenting Lung CT Scans for COVID-19, fast and accurate results are required and furthermore, due to the pandemic, most of the research community has opted for various cloud based servers such as Google Colabs etc to develop their algorithms. High accuracy can be achieved using Deep Networks but the prediction time would vary as the resources are shared amongst many thus requiring the need to compare different lightweight segmentation model. To address this issue, we aim to analyse the segmentation of COVID-19 using four Convolutional Neural Networks (CNN). The images in our dataset are preprocessed where the motion artifacts are removed. The four networks are UNet, Segmentation Network (Seg Net), High-Resolution Network (HR Net) and VGG UNet. Trained on our dataset of more than 3000 images, HR Net was found to be the best performing network achieving an accuracy of 96.24% and a Dice score of 0.9127. The analysis shows that lightweight CNN models perform better than other neural net models when to segment infectious tissue due to COVID-19 from CT slices.

1 Performance Analysis of Lightweight CNN Models to 2 Segment Infectious Lung Tissues of COVID-19 cases 3 from Tomographic Images

4
5 Tharun J Iyer¹, Alex Noel Joseph Raj², Sushil Ghildiyal¹, Nersisson Ruban¹

6
7 ¹ School of Electronics and Electrical Engineering, Vellore Institute of Technology Vellore,
8 Tamil Nadu, India

9 ² Key Laboratory of Digital Signal and Image Processing of Guangdong Province, Department
10 of Electronic Engineering, Shantou University, Shantou, Guangdong, China

11
12 Corresponding Author:

13 Nersisson Ruban¹

14 (Associate Professor, School of Electrical Engineering, Vellore Institute of Technology, Vellore
15 -632014, Tamilnadu, India)

16 Email Address: nruban@vit.ac.in

17 18 Abstract

19 The pandemic of Coronavirus Disease-19 (COVID-19) has spread around the world causing an
20 existential health crisis. Automated detection of COVID-19 infections in the lungs from
21 Computed Tomography (CT) images offers huge potential in tackling the problem of slow
22 detection and augments the conventional diagnostic procedures. However, segmenting COVID-
23 19 from CT Scans is problematic, due to high variations in the types of infections and low
24 contrast between healthy and infected tissues. While segmenting Lung CT Scans for COVID-19,
25 fast and accurate results are required and furthermore, due to the pandemic, most of the research
26 community has opted for various cloud based servers such as Google Colabs etc to develop their
27 algorithms. High accuracy can be achieved using Deep Networks but the prediction time would
28 vary as the resources are shared amongst many thus requiring the need to compare different
29 lightweight segmentation model. To address this issue, we aim to analyse the segmentation of
30 COVID-19 using four Convolutional Neural Networks (CNN). The images in our dataset are
31 preprocessed where the motion artifacts are removed. The four networks are UNet, Segmentation
32 Network (Seg Net), High-Resolution Network (HR Net) and VGG UNet. Trained on our dataset
33 of more than 3000 images, HR Net was found to be the best performing network achieving an
34 accuracy of 96.24% and a Dice score of 0.9127. The analysis shows that lightweight CNN
35 models perform better than other neural net models when to segment infectious tissue due to
36 COVID-19 from CT slices.

37

38

39

40 Introduction

41 During the winter months December 2019, a highly contagious disease outbreak broke in Wuhan,
42 china [1,4]. High grade fever and other flu like symptoms were noticed and most of the patients
43 developed Pneumonia. The pathogen causing the disease was identified as corona virus, and
44 named as Severe Acute Respiratory Syndrome Corona Virus -2 (SARS-CoV-2) [2]. The disease
45 caused by the virus is named by World health Organization (WHO) as Corona Virus Disease
46 (COVID-19). WHO also declared COVID 19 spread as Global public health emergency [2]. As
47 of 9th May 2020, more than 200 countries around the world are affected by COVID-19. There are
48 around 4 million people affected by the disease worldwide with a mortality rate of 6% (around
49 2.75 million people lost their lives). Developed countries like US, Europe and most of the
50 developing countries are suffering a lot from the outbreak. The scientific community is largely
51 involved in devising an antidrug and vaccines for the disease. But unfortunately there are no
52 positive results till date and more over it is reported that, due to mutations, characteristics are
53 changing which makes the vaccine development even more challenging. Taking the situation
54 into account there are very few ways we can control the virus; like staying isolated from the
55 world and breaking the spreading chain of the virus, maintaining the personal hygiene, early
56 detection of the symptoms and taking necessary precautions are few of them.

57

58 The successful control of the outbreak depends on the rapid and accurate detection and
59 identification of the symptoms isolating the patient from the community, so that the spread of the
60 disease can be stopped. Currently, the method used for the detection is Real-time reverse
61 transcriptase polymerase chain reaction (RT-PCR) [5]. It is the standard procedure used by many
62 hospitals and clinics for testing COVID-19 cases. Even though this method remains the reference
63 standard, there are many reported false negative cases using this RT-PCR [8], which is an
64 alarming fact on the situation. It is also time consuming and the limited supply of RT-PCR kits
65 for the rural areas make the testing more difficult [6]. Since the COVID-19 patients develop
66 breathe related discomfort and Pneumonia as the outcome of the disease progress, Radiological
67 studies can play a vital role in diagnosing the lung infections caused by this episode [9]. The CT
68 chest scan can be used to identify the early stages of lung infections and related problems. The
69 chest CT reveals the initial pulmonary abnormalities for COVID-19 patients for whom RT-PCR
70 gave negative results [3].

71

72 The common manifestations of SARS-CoV-2 in chest CT scan are:- ground glass opacities,
73 consolidation, crazy paving, dilation of vessel width in some cases and round shape lesions in
74 few cases [7,9]. The effectiveness of the chest CT scan based COVID-19 management depends
75 on the efficient automatic detection and segmentation of regions in the scan. So in that context
76 the recent developments in the imaging technologies come handy. There are plenty of imaging
77 tools which give very high and accurate quantification of abnormal conditions. This procedure of
78 image based diagnosis system involves capturing the image, analysing the image by a trained,
79 experienced radiologist and annotation is made for the ground truth segments. The current

80 scenario slows down the annotation of the images, labelling and getting the ground truth
81 processes due to the increasing number of patients day by day, lack of radiologist and the over
82 duty burden of existing radiologists. So automatically detecting the infected regions from the
83 chest CT scan using computer based algorithms are the current trends in research that gives
84 wonderful results and aids in medical diagnostics.

85

86 The main objective of the research work is comparing the segmentation performance of
87 computationally non-intensive models deep learning model when subjected to Lung CT Scans
88 for that are affected by COVID-19 a. The models utilized for the research belong to the U-Net
89 variants models which are the most popular models of choice for segmentation of Medical
90 Images. Here we compare the traditional U-Net model as proposed by Ronneberger with other
91 variants such as Seg Net, U-Net based on VGG16 and HR-Net (High Resolution Net) and
92 present both qualitative and quantitative results.

93

94 **Materials & Methods**

95 The Block diagram describing the entire methodology is shown below in Figure 1. The
96 description of each method is described below.

97 **Dataset Considered:**

98 The dataset used consists of 3770 images and their corresponding ground truths. 3020 training
99 images are used and 750 testing images are used. The CT scans of 50 patients were taken from
100 mosmed.ai [19] were openly accessible Neuroimaging Informatics Technology Initiative (NIFTI)
101 images were provided. The data was collected from the Research and Practical Clinical Center
102 for Diagnostics and Telemedicine Technologies of the Moscow Health Care Department. The
103 CT Scans were obtained between 1st March 2020 and 25th April 2020. Each NIFTI file was
104 decompressed to PNG images and used for the study. The CT scans of another 20 patients were
105 taken from zenodo.org [20] where the NIFTI files of 20 patients were provided. The images were
106 annotated by two radiologists and verified by an experienced radiologist. For both datasets,
107 MATLAB was used to extract the PNG images.

108

109 **Pre-Processing:**

110 The images in the dataset are riddled with motion artefacts and noise. Motion artefacts are
111 caused due to improper imaging techniques and are a specific kind of noise relevant to CT Scans.
112 Therefore, removing this noise is important or else it will cause the algorithms to learn
113 improperly. MATLAB is used to remove the noise and motion artefacts. The original image is
114 converted to grayscale from RGB and then, the image properties are extracted. Area and Solidity
115 are used and then, the image is thresholded after selecting the max area and highest solidity.
116 Once a mask is ready, the mask is multiplied with the original image to get the pre-processed
117 image. A comparison is given below in Figure 2. As can be seen, motion artefacts are removed
118 and the image has more clarity.

119

120 HR Net:

121 HRNet is developed at Microsoft and has signified state of art presentation in the areas of
122 semantic segmentation, image classification, facial detection, object detection and pose
123 estimation [10]. Its attention is on training High Resolution (HR) representation. The existing
124 techniques recuperate representation of high resolution from representation of low resolution
125 formed by high to low resolution network. In HRNet, from first stage commencement high-
126 resolution network, progressively augment high to low resolution networks successively to
127 arrange more steps and associate the multi-resolution network in parallel.

128

129 HRNet is able of uphold high-resolution representation throughout the process as repeated multi-
130 scale combinations are conducted by switching the information through the multi-resolution
131 parallel subnetworks repeatedly throughout the process [11]. The architecture of resulting
132 network is displayed in Figure 3. This network has advantages in contrast to existing networks
133 like Segnet, UNET, Hourglass etc. These existing networks lose a lot of essential information in
134 the progression of recovering high-resolution from low-resolution representation. HRNet links
135 high to low resolution networks in parallel instead of series and this gives high-resolution
136 representation throughout the process, correspondingly the estimated heatmap is much accurate,
137 spatially much precise.

138

139 Multi-resolution sequential subnetwork

140 Existing models works by linking high to low resolution convolutions subnetwork in series,
141 where each individual subnetwork form a platform, collection of an arrangement of convolutions
142 furthermore, there is a down sample layer through end-to-end subnetworks to split the resolution
143 into halves.

144 Let \mathcal{N}_{sr} be the subnet in the stage s^{th} and resolution index r . First subnet resolution is given by

145 $\frac{1}{2^r - 1}$. The high-to-low system with S phases/stages (I.e.: 4) can be indicated as:

146

147

$$148 \quad \mathcal{N}_{11} \rightarrow \mathcal{N}_{22} \rightarrow \mathcal{N}_{33} \rightarrow \mathcal{N}_{44} \quad (1)$$

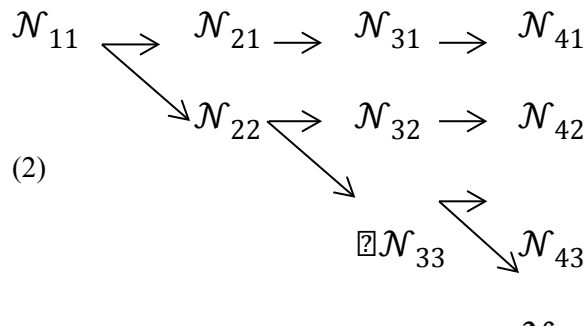
149

150 Multi-resolution parallel subnetwork

151 Starting from first phase/stage begin with high resolution subnet, slowly enhance high to low
152 resolution subnet, generating new phases/stages, and associate multi-resolution subnet in
153 parallel. Eventually, the parallel subnet resolution of a later phase/stage comprises of the
154 resolution from an earlier stage and below one stage. The network shown below contains 4
155 parallel subnets.

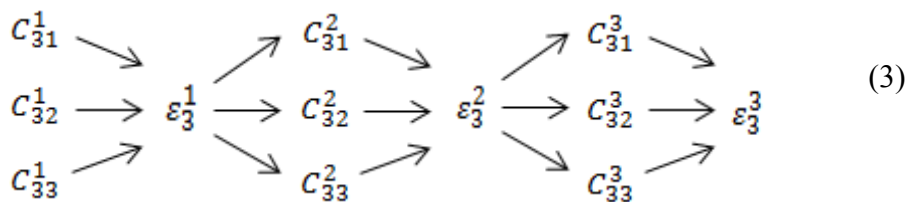
156

157



167 Multi-scale repeated fusion

168 In this network exchange units were introduced throughout parallel subnet in such a way that an
169 individual subnet continuously collects information from parallel subnets. How information is
170 exchanged lets understand this process through an example here third stage is subdivided into
171 multiple exchange blocks and every block consists of three parallel convolution modules, having
172 exchange units followed by parallel units which is shown below,



181 Where:

182 C_{sr}^b – Convolution module,

183 ϵ_s^b – Exchange Unit,

184 and s is the stage, r is the resolution and b is the block

185
186
187 Explanation of exchange units is show in Figure 4. The input mapping is given by : $\{X_1, X_2, X_3,$
188 $\dots, X_s\}$ and the output mapping was given by: $\{Y_1, Y_2, Y_3, \dots, Y_s\}$. The width and resolution of
189 the output is same as input. Every output is a sum of input mapping i.e $Y_K = \sum_{i=1}^s a(X_i, K)$.

190 Assume of 3×3 stride was done for down sampling and for up sampling 1×1 convolution
191 (nearest neighbor).

192 HRNet experimental results (when tested with different datasets) show remarkable results for the
193 applications like facial detection, semantic segmentation, and object detection.

194 195 Seg Net:

196 At the university of Cambridge, UK, team of the robotics group researched and developed that
197 SegNet is a deep encoder decoder architecture for multiclass pixel-wise segmentation [12]. The
198 framework comprises order of non-linear processing layers which is called encoders and a
199 similar set of decoders afterward a pixel wise classifier. Generally, encoder have made up of a
200 ReLU non-linearity and one or more convolutional layers with batch normalization, subsequently
201 non-overlapping maxpooling and subsampling. Using Max-pooling indices in encoding
202 sequence, for up sampling the sparse encoding in consequence the pooling process to the
203 decoder. Use of max-pooling indices in the decoders is the one important feature of the SegNet
204 to execute the sampling of low resolution maps. For segmented images the tendency to retain
205 high frequency details and capable enough to decrease the number of parameters in the decoder
206 needed for training are some advantages of SegNet. Using stochastic gradient descent this
207 framework can be trained end-to-end.

208

209 SegNet is composed of encoder and decoder after a last pixel-wise classification layer. The
210 architecture is shown in Figure 5. The encoder in SegNet is composed of convolution layers
211 which are 13 in number, and these layer matches with the 13 starting layers of VGG16,
212 considered for classifying the objects [13].

213

214 Figure 6 illustrates the decoding method utilized by SegNet in which there is no learning
215 engaged with the up-sampling stage. The upsampling of decoder network's feature map (input) is
216 done by learned maxpooling indices from the equivalent encoder feature map. Dense feature
217 maps are generated by combining feature maps and trainable decoder channel.

218

219 SegNet a deep network was used for semantic segmentation. Basically, It was designed because
220 the motivation behindhand was to propose an architecture for roads, outdoor and indoor sites
221 which is proficient together in terms of computational time and memory. Feature map's
222 maxpooling indices are only stored in SegNet and to attain better performance it uses them in its
223 decoder network.

224

225 **UNet:**

226 The UNet design is based upon the fully convolution network and adjusted such that it produces
227 better segmentation results in medical imaging. UNet consists of two paths named as contracting
228 and and expansive. In the contracting path it captures the context whereas in expansive path it
229 enables exact localization. While contracting path is a classical architecture of UNet. It includes
230 two 3x3 convolutions, max pooling operation with repeating application. The Figure 7 illustrates
231 the architecture of UNet, which is U in shape that itself gives the name 'UNet'. The main
232 philosophy behind this network is, it replace pooling operation by using upsampling operators
233 [14]. So, ultimately the resolution will increase layer by layer. The main feature of UNet is the
234 large number of channels which lead to higher resolution. Moreover, in every downsampling it
235 doubles the feature channels.

236

237 Each stage in the expansive path involves upsampling of the feature channel followed by (2x2)
 238 convolution that splits the number of feature channels into halves. In contracting path, it crops
 239 the feature map because of loss in border pixel in each convolution. Final layer is mapped by 1x1
 240 convolutions which is used to map all 64 units feature vector. The network contains total 23
 241 convolutional layers. UNet performs well on image segmentation [15].
 242 While training the UNet model, the cross- entropy loss function united with the last feature map
 243 and by applying a pixel- wise softmax over it, the softmax is denoted as:

$$244 \quad p_k = \frac{e^{(a_k(x))}}{\sum_{k=1}^K e^{(a_k(x))}} \quad (4)$$

245
 246 In addition, the energy function is calculated by:

$$247 \quad E = \sum_{x \in \Omega} w(x) \log(p_{l(x)}(x)) \quad (5)$$

248 Where:

249 a_k : Represents the activation in feature map k

250 p_k : Represents estimated maximum function

251 K: No. of class

252 $x \in \Omega$: Pixel position

253 $p_{l(x)}$: Deviation

254 In the training data set, to counterbalance the diverse frequency of pixels from a specific class
 255 the weight map is pre calculated for ground- truth segmentation, and enforcing the network to
 256 study the minor separation borders amid touching cells introduce by us.

257 The morphological operation used to calculate separation borders, the weight map calculated
 258 using:

$$259 \quad w(x) = w_c(x) + w_0 \cdot e^{-\frac{(d_1(x) + d_2(x))^2}{2\sigma^2}} \quad (6)$$

260 Where:

261 w : denotes the weight map

262 d_1 : distance upto border of nearest first cell

263 d_2 : distance upto border of nearest second cell

264

265 VGG UNet:

266 Image segmentation, which is performed pixel wise is most preferable task in the field of
 267 computer vision. Encoders- decoders when combined they form UNET architectures, which are
 268 very famous for image segmentation in medical imaging and satellite images etc. The weights of
 269 the pre-trained models (like ImageNet) are used to initialize the weights of the neural network
 270 (i.e trained on large dataset) as it gives better performance major than those models, which are
 271 trained on small dataset from scratch. Models accuracy is very important in some applications
 272 like traffic safety and medicine pre-trained encoder can enhance the architecture and
 273 performance of UNET. Applications like Object detection, image classification and scene

274 understanding have improved their performance after the introduction of convolutional neural
275 network (CNN). Nowadays, CNN has outperformed in several fields over human experts.

276

277 Image segmentation plays vital role in the field of medical imaging to enhance the diagnostic
278 capabilities. Fully connected network (FCN) is amongst the most popular state- of-the-art
279 machine learning technique [16]. Segmentation accuracy attained by some advancement in

280

281 FCN as compared to PASCAL VOC [17] common approach on standard datasets

282 UNet consists of two paths named as contracting and and expansive. In the contracting path it
283 captures the context whereas in expansive path it enables exact localization. The contracting path
284 sticks with the design of a convolutional network with pooling operations, alternating
285 convolution, gradually down sample feature channels and expanding many feature maps\ layer
286 simultaneously, each stage in the expansive path composed of an up-sampling of the feature
287 channel along with a convolution. The VGGUnet architecture is illustrated in Figure 8. The
288 encoder for UNET model is composed of 11 successive (series) layers VGG family and denoted
289 by VGG-11 [3]. VGG-11 consist of 7 convolution layers each using rectified linear unit (ReLU)
290 activation function, 5 maxpooling operations each reduces feature channel by 2 and the kernels
291 size 3x3 is used for every convolutional layer [18].

292 Common loss function i.e binary cross entropy can be used for classification problem where \hat{y}_i
293 denotes the prediction, y_i denotes the true value and m denotes the no. of samples

294

$$295 \quad H = -\frac{1}{m} \sum_{i=1}^m (y_i \log \hat{y}_i + (1 - y_i) \log (1 - \hat{y}_i)) \quad (7)$$

296

297 **Performance Validation:**

298 To validate the performance of the models presented above, Sensitivity, Specificity, Jaccard
299 Index, Dice Coefficient, Accuracy and Precision are used. To measure the accuracy of the
300 segmented image, accuracy and precision are used and to measure the quality of segmentation,
301 sensitivity and specificity are used. The various performance measures are described below:
302 Accuracy and Precision are used to calculate the accuracy of the segmentation model itself.
303 Accuracy is as the ratio of correct predictions to the total number of predictions and Precision is
304 defined as the ratio of correctly predicted positive observations to the total number of correctly
305 predicted observations.

$$306 \quad Accuracy = \frac{TP + TN}{TP + TN + FP + FN} \quad (8)$$

$$307 \quad Precision = \frac{TP}{TP + FP} \quad (9)$$

308 In the case of segmentation, accuracy and precision are used to measure the binary segmentation
309 of each pixel of the image by the model. Although precision and accuracy may seem to be
310 enough to describe the performance of the model, other factors are also important to describe the
311 quality of segmentation.

312

313 Sensitivity and Specificity are used to measure the quality of segmentation between the classes.
314 In this case, the models are performing binary segmentation. So, Sensitivity, or the True Positive
315 Rate, measures the quality of segmentation of one class and Specificity, or the True Negative
316 Rate, measures the quality of segmentation of the other class. Sensitivity and Specificity can be
317 defined as:

$$318 \quad \text{Sensitivity} = \frac{TP}{(TP + FN)} \quad (10)$$

$$319 \quad \text{Specificity} = \frac{TN}{(TN + FP)} \quad (11)$$

320 With Sensitivity and Specificity, having a high value for each is good as it shows that the model
321 is able to segment the pixels correctly without any errors.

322

323 The Jaccard Index and Dice Coefficient are used to quantify the similarity between the original
324 image and the segmented image. Jaccard Index and Dice Coefficient are similar to the
325 Intersection over Union (IoU) used to evaluate Object detection models. Jaccard Index and Dice
326 Coefficient ranges from 0 to 1 where 0 means no overlap and 1 mean full similarity. Jaccard
327 Index and Dice Coefficient can be defined as:

$$328 \quad \text{Dice Coefficient} = \frac{2TP}{2TP + FP + FN} \quad (12)$$

$$329 \quad \text{Jaccard Index} = \frac{TP}{TP + FP + FN} \quad (13)$$

330 While the Dice coefficient and the Jaccard Index are quite similar, ideally, the two measures
331 have to be equal. So, to measure the quality of similarity of the model, a similarity between the
332 Dice Coefficient and Jaccard Index can be viewed to measure the quality of segmentation.

333

334 **Results and Discussion**

335 The experiments were conducted in the Google Colab platform. As shown in Table 1, HR Net is
336 shown to have the highest performance as compared to the other models. The second best model
337 is the classical UNet, the third best model is the VGG UNet and the model with the worst
338 performance is the Seg Net. The reason for the high performance of the HR Net is the fact that
339 the HR Net extracts high resolution information and retains in throughout the segmentation
340 process. This is due to the parallel networks that are able to maintain essential information. HR
341 Net indicates a high accuracy of segmentation with an Accuracy of 0.9624 and a Specificity of
342 0.9930.

343

344 Figure 9. shows the various outputs obtained from the models which segmented the test image.
345 HR Net shows the best segmentation performance while UNet shows good performance too.
346 UNet is able to obtain a proper boundary similar to the test image. Seg Net has performed poorly
347 to segment the image. Neither has it obtained a boundary nor has it segmented the finer details
348 properly. The VGG UNet has segmented the image properly but not to the extent of HR Net or
349 UNet. We can see that HR Net has the best performance. With decreased area, the performance

350 decreases which means that UNet is the second best performance, VGG UNet is the third best
351 and Seg Net has the worst performance amongst the models.

352

353 From Figure 10, we can infer that the performance of the HR Net is the best as it has the greatest
354 area. The 6 points are the performance measures namely, Sensitivity, Specificity, Precision,
355 Accuracy, Jaccard Index and Dice Coefficient. The glyph plot is a good way to directly compare
356 the performance of various models through the use of polygons.

357

358 As can be seen from Table 2, HR-Net has the highest number of layers at 1043 with other
359 models having less than 100 layers. But, HR-Net has similar parameters to VGG UNet and an
360 even lesser number of parameters than SegNet. This is due to the architecture of the HR-Net. It is
361 able to extract deeper features than the other models while maintaining the overall file size and
362 number of parameters. The reason for HR-Net having the highest performance is its architecture
363 which makes it the best model to be used for fast inference. Comparing the SegNet, VGG UNet
364 and UNet, SegNet has the poorest inference speed at 84 ms with the largest model size. It is
365 therefore inferred that SegNet is the worst model to use for the Segmentation of COVID-19
366 based on our study. VGG UNet and UNet have different metrics due to the fact that VGG UNet
367 is trained on the VGG-16 weights. It, therefore, takes far higher time to load on and produce an
368 inference than UNet. If HR-Net cannot be used, VGG UNet is the next best network for
369 segmenting COVID-19.

370

371 **Conclusion**

372 In this paper, we analyzed four models for segmenting COVID-19 from Lung CT Images. With
373 the growing number of cases worldwide, quick and accurate testing is needed. To solve this
374 problem, we approached the problem by reviewing four lightweight models that do not take a
375 long time for training or testing. First, we remove motion artefacts from the tomographic images
376 through Thresholding and use the pre-processed images for training the models. The four models
377 trained are Seg Net, UNet, VGG UNet and HR-Net. We evaluate the models on their
378 performance using accuracy, dice, Jaccard index and precision. We also used Specificity and
379 Sensitivity as secondary evaluation characteristics. The results obtained demonstrate that
380 lightweight convolutional networks have high latent ability to segment COVID-19 from CT
381 images with HRNet being the best network out of the four models analysed. In the future, we
382 will increase the number of CT images by collaborating with hospitals and multi-centre
383 collaborations.

384

385 **Acknowledgements**

386 We would like to thank VIT University for the nurturing environment as well as the exposure it
387 provided for us to complete this project. We also would like to thank MosMedData for the Covid
388 19 dataset which is used for this research work.

389

390 **References**

- 391 1. Zhu N, Zhang D, Wang W et al. A Novel Coronavirus from Patients with Pneumonia in
392 China, 2019. *The New England journal of medicine* 2020; 382: 727–733.
- 393 2. World health Organization: WHO Director General’s remarks at the media briefing on
394 2019-n CoV on 11th February 2020. At: [https://www.who.int/dg/speeches/detail/who-](https://www.who.int/dg/speeches/detail/who-director-general-s-remarks-at-the-media-briefing-on-2019-ncov-on-11-february-2020)
395 [director-general-s-remarks-at-the-media-briefing-on-2019-ncov-on-11-february-2020](https://www.who.int/dg/speeches/detail/who-director-general-s-remarks-at-the-media-briefing-on-2019-ncov-on-11-february-2020).
396 Published February 11, 2020.
- 397
- 398 3. Ai, T., Yang, Z., Hou, H., Zhan, C., Chen, C., Lv, W., Tao, Q., Sun, Z. and Xia, L., 2020.
399 Correlation of chest CT and RT-PCR testing in coronavirus disease 2019 (COVID-19) in
400 China: a report of 1014 cases. *Radiology*, p.200642.
- 401 4. Liu, W., Zhang, Q., Chen, J., Xiang, R., Song, H., Shu, S., Chen, L., Liang, L., Zhou, J.,
402 You, L. and Wu, P., 2020. Detection of Covid-19 in children in early January 2020 in
403 Wuhan, China. *New England Journal of Medicine*, 382(14), pp.1370-1371.
- 404 5. Li, Y. and Xia, L., 2020. Coronavirus disease 2019 (COVID-19): role of chest CT in
405 diagnosis and management. *American Journal of Roentgenology*, pp.1-7.
- 406 6. Chen, X., Yao, L. and Zhang, Y., 2020. Residual Attention U-Net for Automated Multi-
407 Class Segmentation of COVID-19 Chest CT Images. *arXiv preprint arXiv:2004.05645*.
- 408 7. Hamer, O.W., Salzberger, B., Gebauer, J., Stroszczyński, C. and Pfeifer, M., 2020,
409 March. CT morphology of COVID-19: Case report and review of literature. In *RöFo-*
410 *Fortschritte auf dem Gebiet der Röntgenstrahlen und der bildgebenden Verfahren*. ©
411 Georg Thieme Verlag KG.
- 412 8. Chan JF, Yuan S, Kok KH, et al. A familial cluster of pneumonia associated with the
413 2019 novel coronavirus indicating person-to-person transmission: a study of a family
414 cluster. *Lancet*. 2020 Jan 24. pii: S0140-6736(20)30154-9. doi: 10.1016/S0140-
415 6736(20)30154-9. [Epub ahead of print]
- 416 9. Zu, Z.Y., Jiang, M.D., Xu, P.P., Chen, W., Ni, Q.Q., Lu, G.M. and Zhang, L.J., 2020.
417 Coronavirus disease 2019 (COVID-19): a perspective from China. *Radiology*, p.200490.
- 418 10. Sun, K., Xiao, B., Liu, D., & Wang, J. (2019). Deep high-resolution representation
419 learning for human pose estimation. *Proceedings of the IEEE Computer Society*
420 *Conference on Computer Vision and Pattern Recognition*, 2019-June, 5686–5696.
- 421 11. Sun, K., Zhao, Y., Jiang, B., Cheng, T., Xiao, B., Liu, D., ... Wang, J. (2019). High-
422 Resolution Representations for Labeling Pixels and Regions.
- 423 12. Badrinarayanan, V., Kendall, A., & Cipolla, R. (2017). SegNet: A Deep Convolutional
424 Encoder-Decoder Architecture for Image Segmentation. *IEEE Transactions on Pattern*
425 *Analysis and Machine Intelligence*, 39(12), 2481–2495.
- 426 13. Mannem, R., Ca, V., & Ghosh, P. K. (2019). A SegNet based image enhancement
427 technique for air-tissue boundary segmentation in real-time magnetic resonance imaging
428 video. 25th National Conference on Communications, NCC 2019.

- 429 14. Ronneberger, O., Fischer, P., & Brox, T. (2015). U-net: Convolutional networks for
430 biomedical image segmentation. Lecture Notes in Computer Science (Including Subseries
431 Lecture Notes in Artificial Intelligence and Lecture Notes in Bioinformatics), 9351, 234–
432 241.
- 433 15. Livne, M., Rieger, J., Aydin, O. U., Taha, A. A., Akay, E. M., Kossen, T., Madai, V. I.
434 (2019). A U-net deep learning framework for high performance vessel segmentation in
435 patients with cerebrovascular disease. *Frontiers in Neuroscience*, 13(FEB), 1–13.
436 <https://doi.org/10.3389/fnins.2019.00097>
- 437 16. J. Long, E. Shelhamer and T. Darrell. Fully Convolutional Networks for Semantic
438 Segmentation. Proceedings of the IEEE Conference on Computer Vision and Pattern
439 Recognition. 2015.
- 440 17. M. Everingham, et al. The Pascal Visual Object Classes Challenge: A Retrospective.
441 *International Journal of Computer Vision* 111, 98-136, 2015.
- 442 18. Igloukov, V., & Shvets, A. (2018). TerausNet: U-Net with VGG11 Encoder Pre-
443 Trained on ImageNet for Image Segmentation. Retrieved from
444 <http://arxiv.org/abs/1801.05746>.
- 445 19. Morozov, S.P., Andreychenko, A.E., Pavlov, N.A., Vladzimirskyy, A.V., Ledikhova,
446 N.V., Gomboleviskiy, V.A., Blokhin, I.A., Gelezhe, P.B., Gonchar, A.V. and Chernina,
447 V.Y., 2020. MosMedData: Chest CT Scans with COVID-19 Related Findings Dataset.
448 *arXiv preprint arXiv:2005.06465*.
- 449 20. Ma Jun, Ge Cheng, Wang Yixin, An Xingle, Gao Jiantao, Yu Ziqi, He Jian. (2020).
450 COVID-19 CT Lung and Infection Segmentation Dataset (Version Verson 1.0) [Data
451 set]. Zenodo. <http://doi.org/10.5281/zenodo.3757476>

Figure 1

Comparison between original image and pre-processed image

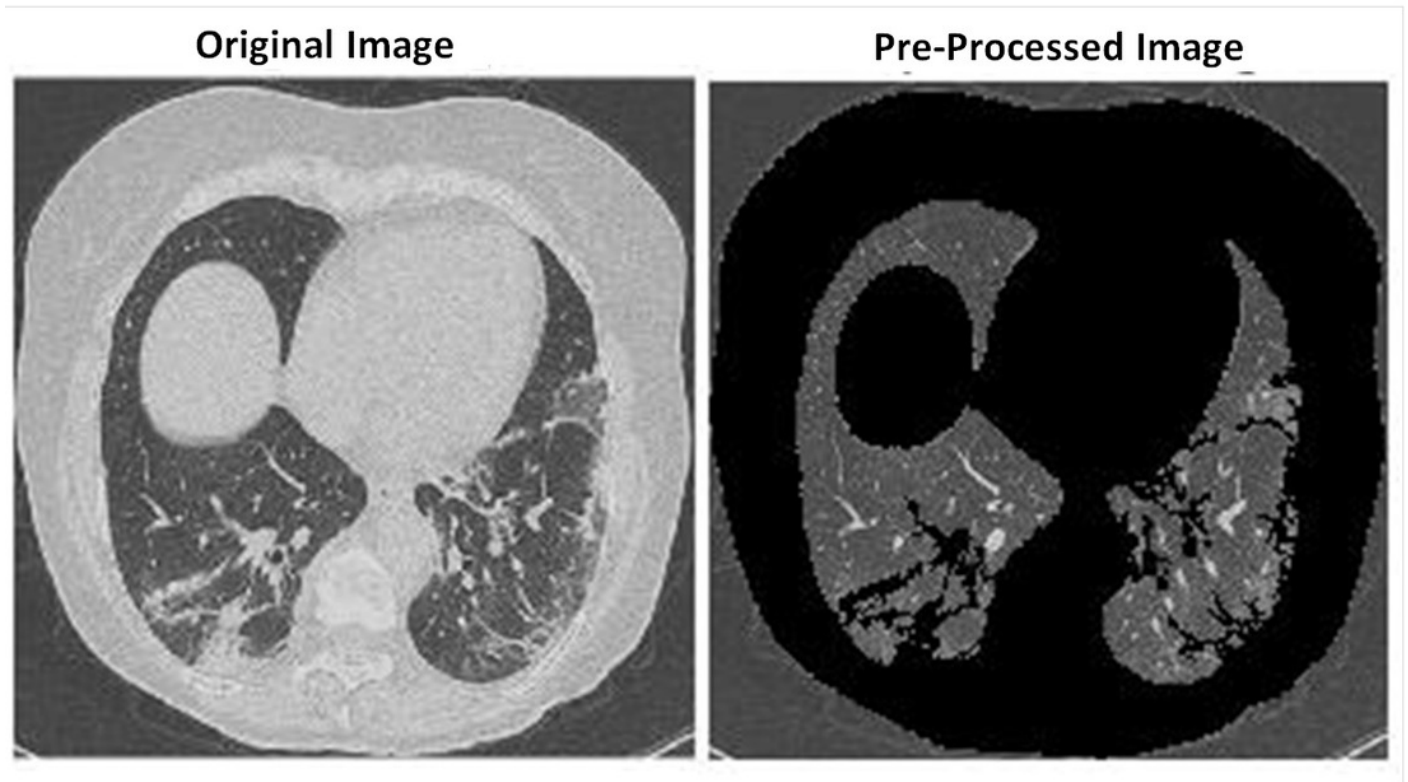


Figure 2

Block Diagram of proposed method

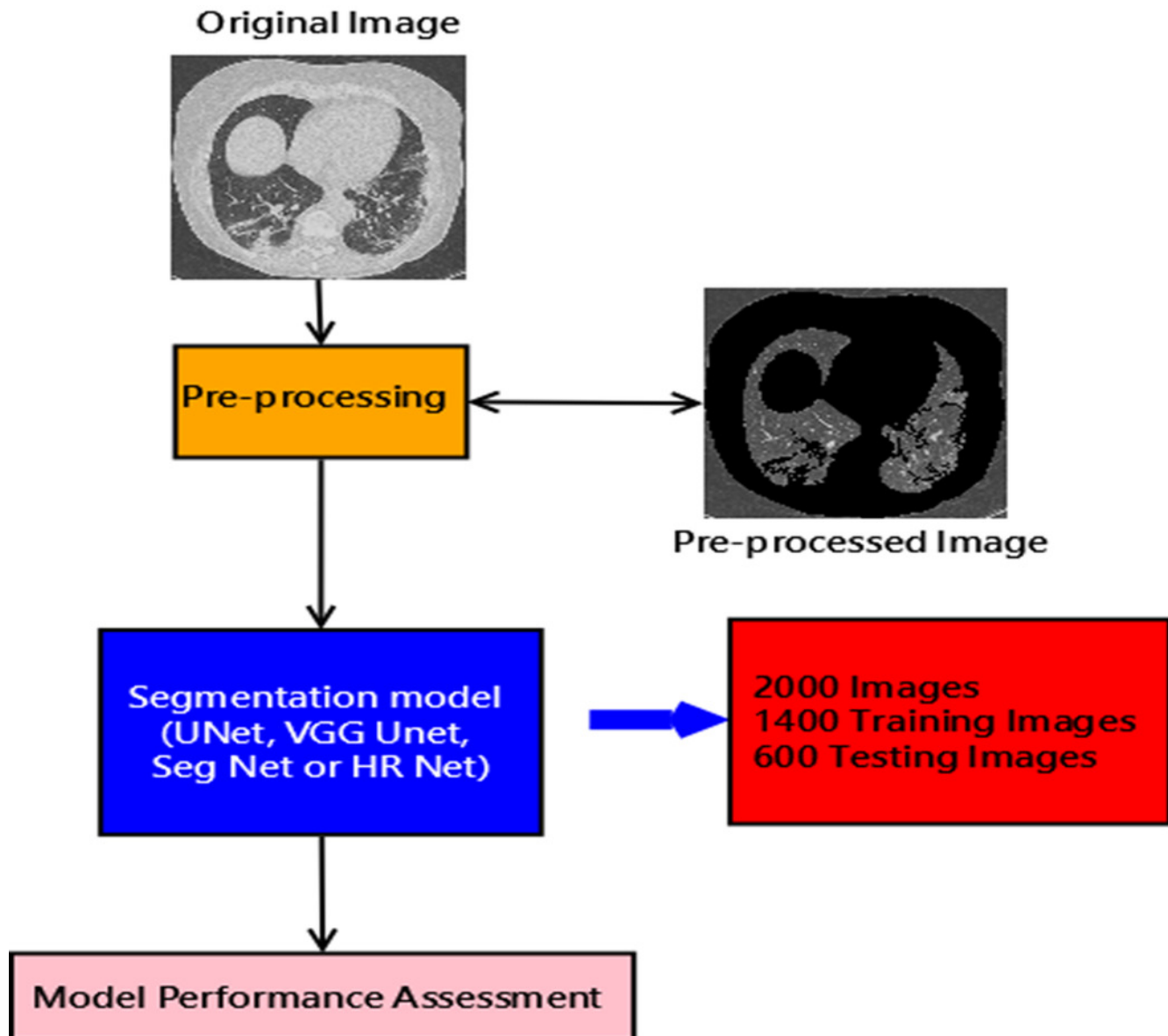


Figure 3

Architecture of HRNet

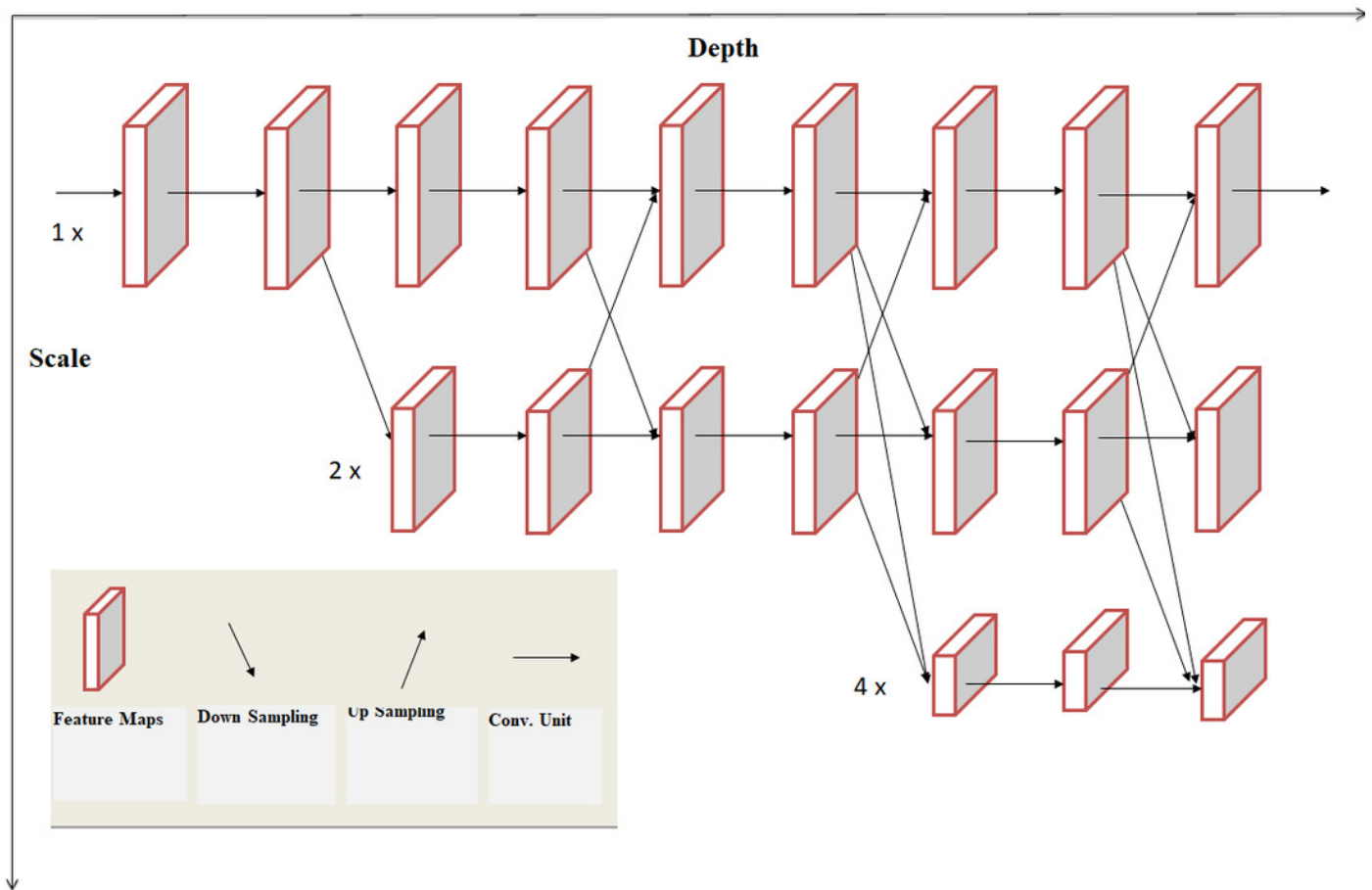


Figure 4

Low, Medium and High resolution (left to right)

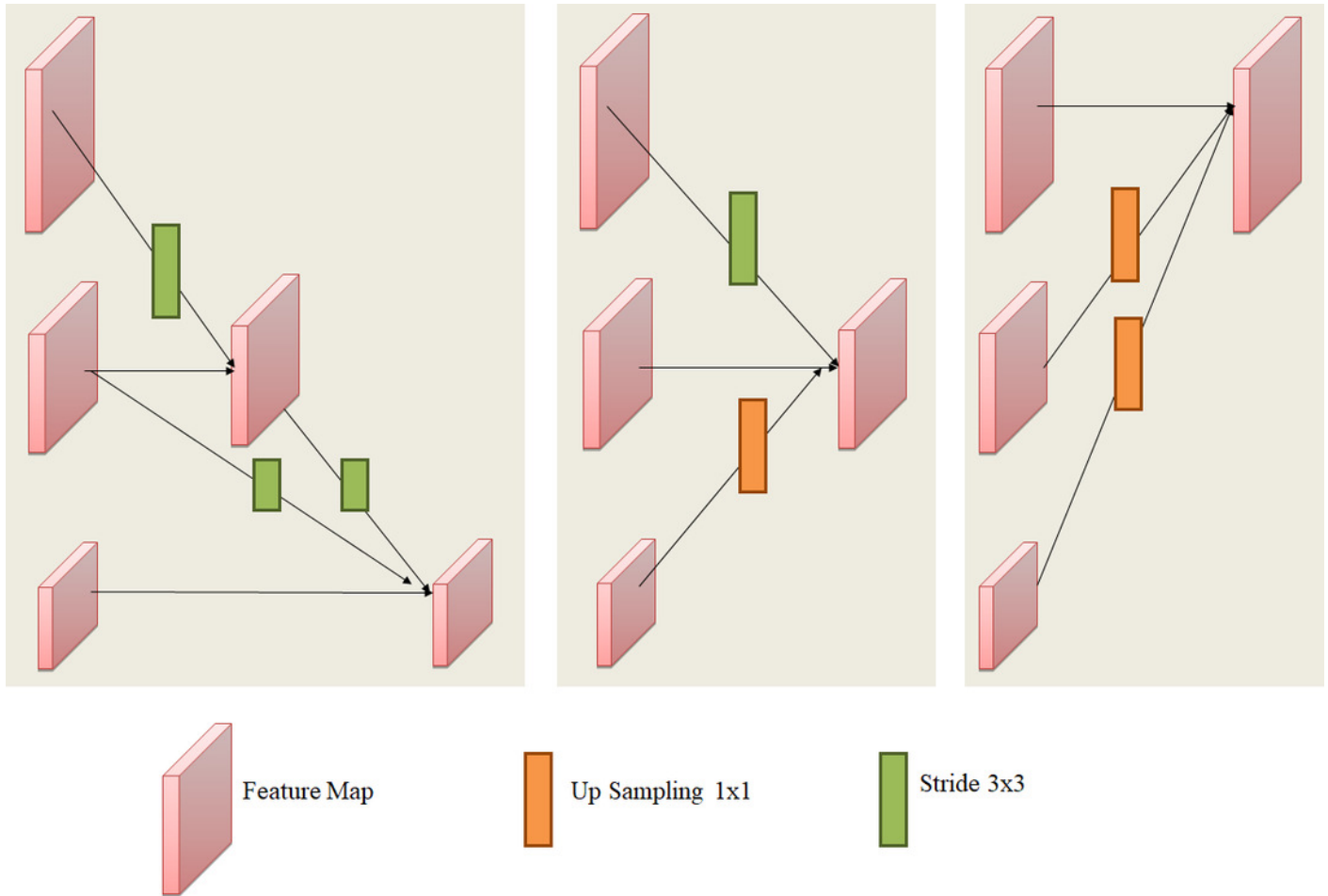


Figure 5

SegNet Architecture

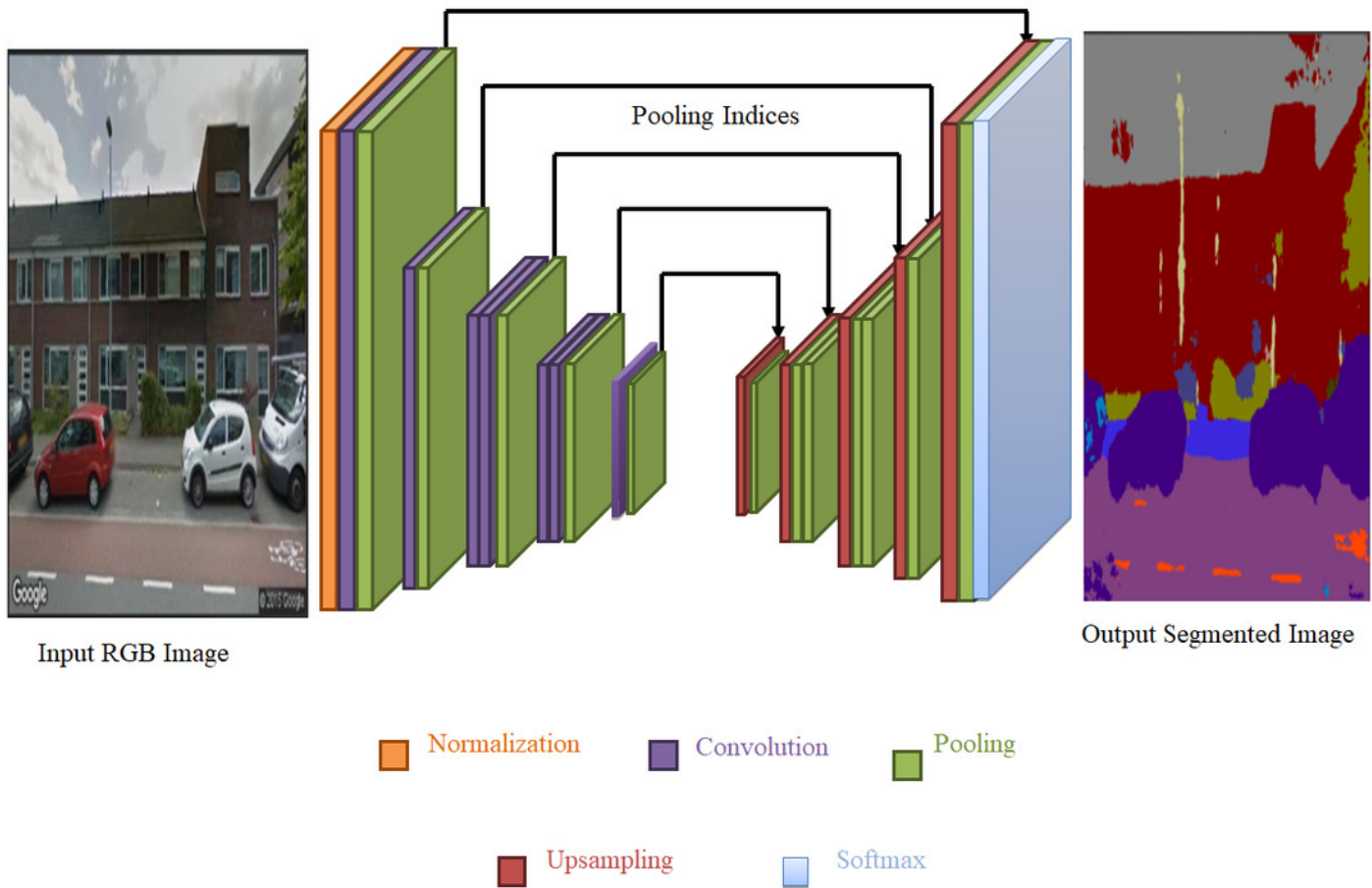


Figure 6

Decoding Techniques used by SegNet

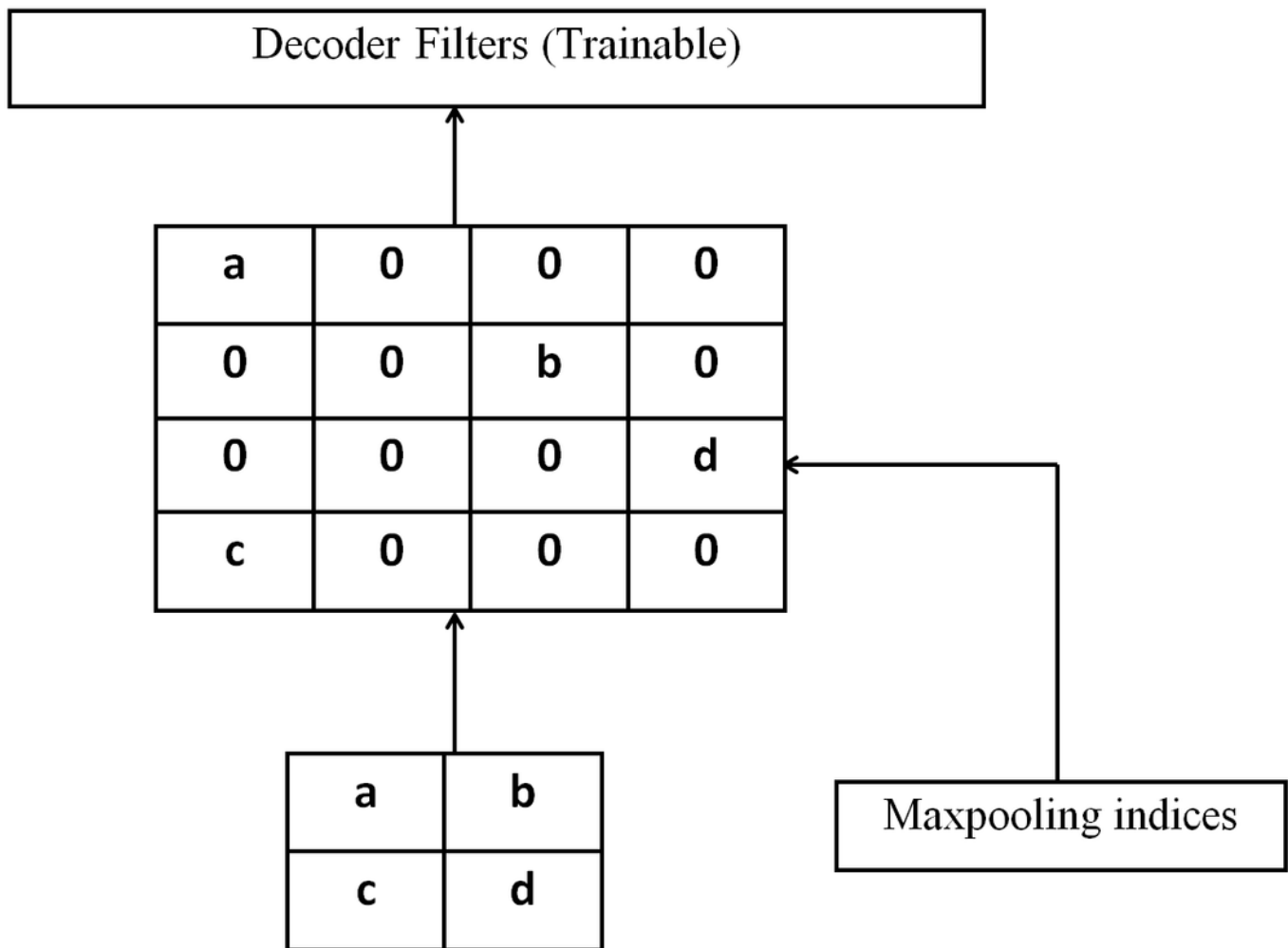


Figure 7

Illustrating the architecture of U-Net

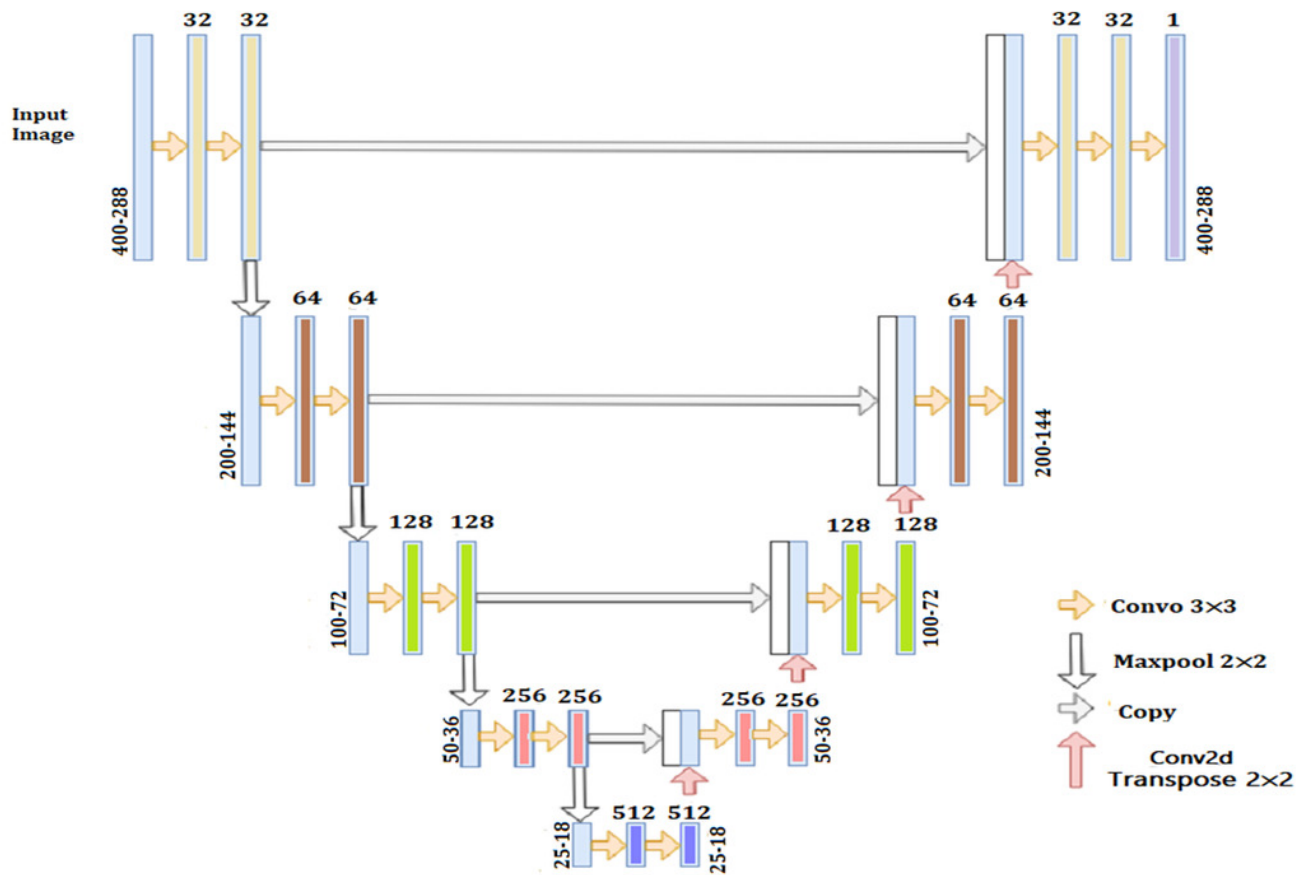


Figure 8

Illustrating encoder decoder architecture also known as VGGUNet

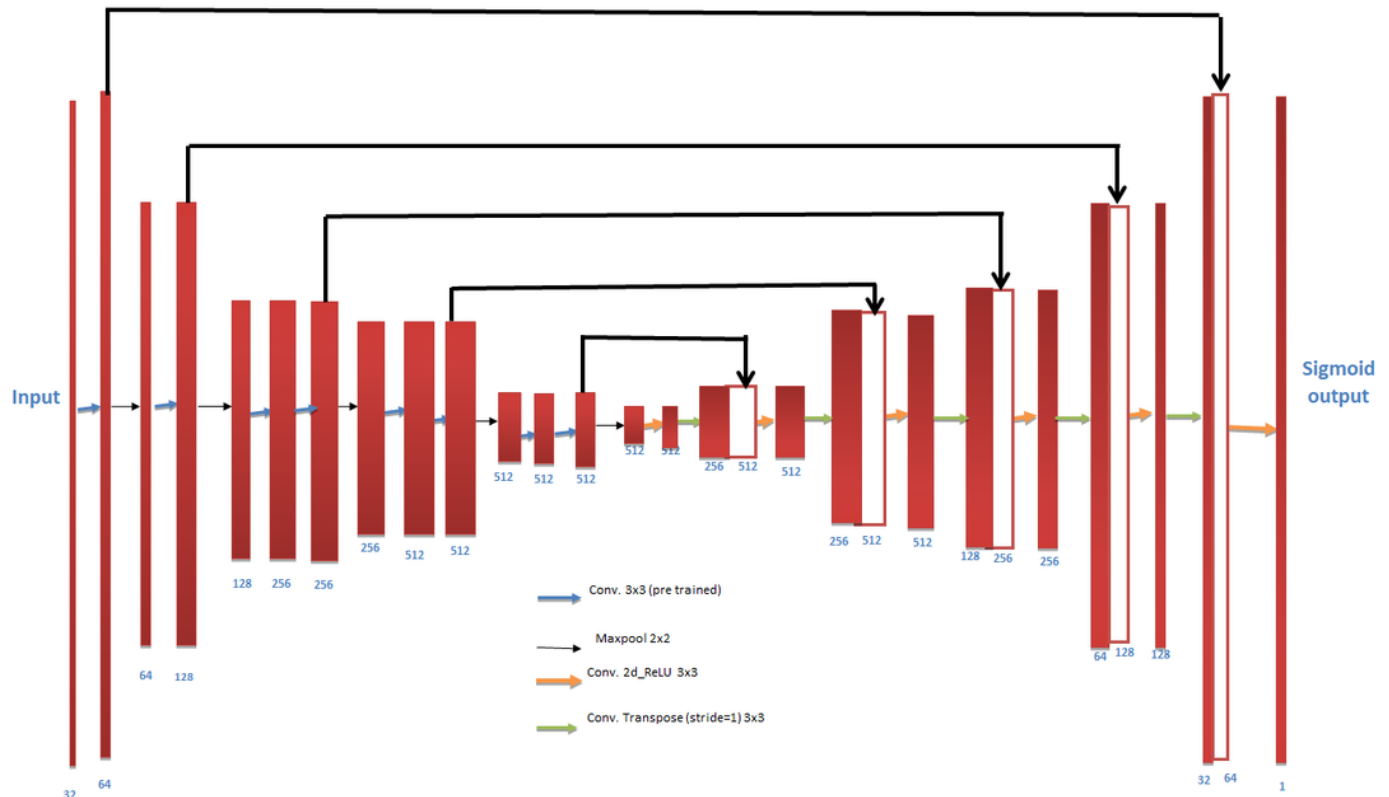


Figure 9

Sample test image and corresponding results obtained with the proposed method: (a) Original test Image after the artifact removal; (b) Binary image; (c) Region of Interest; (d)-(g) Segmentation results obtained with HR-Net, Seg Net, UNet, and VGG Net resp

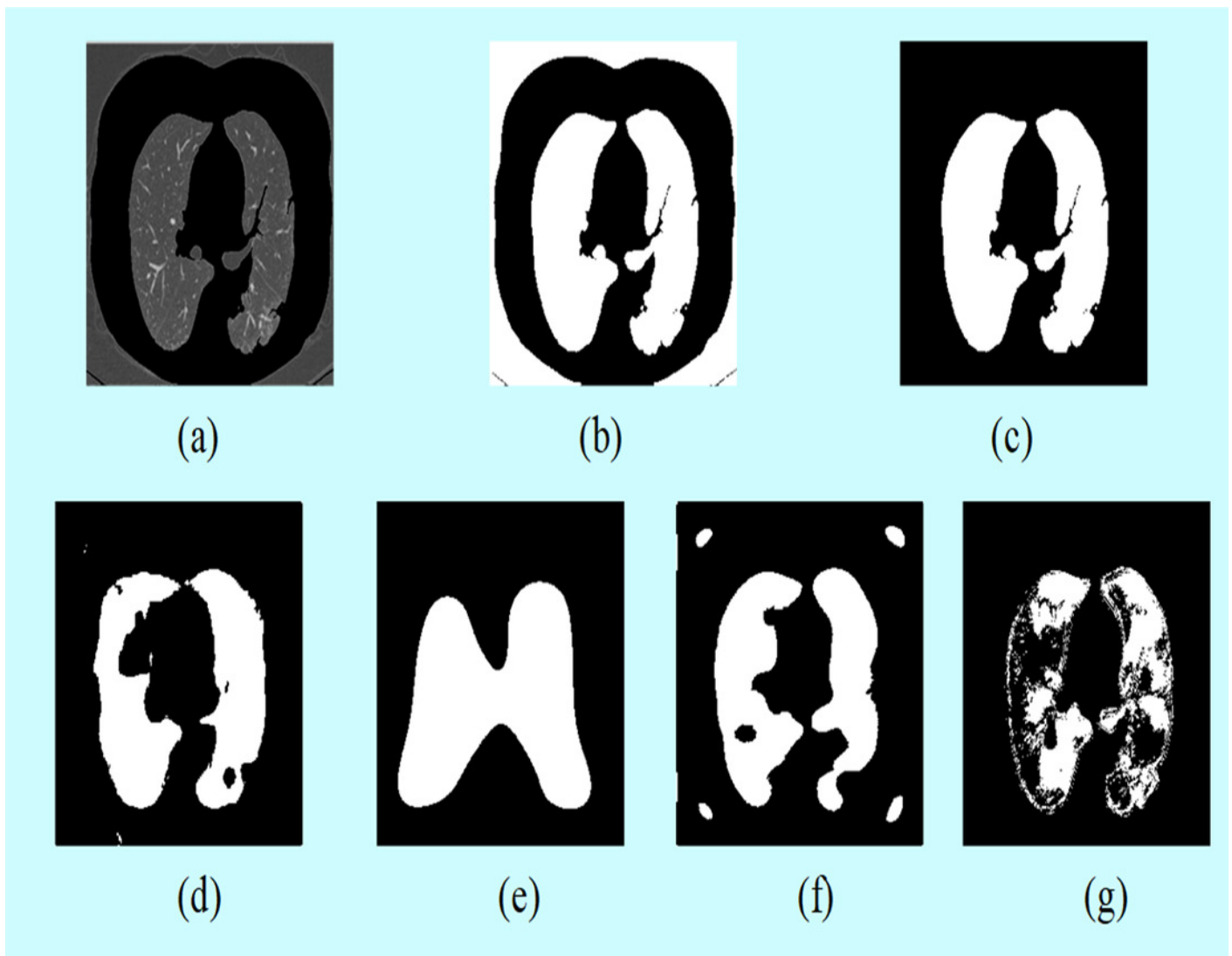


Figure 10

Glyph plot representing the performance of the models over the performance measures

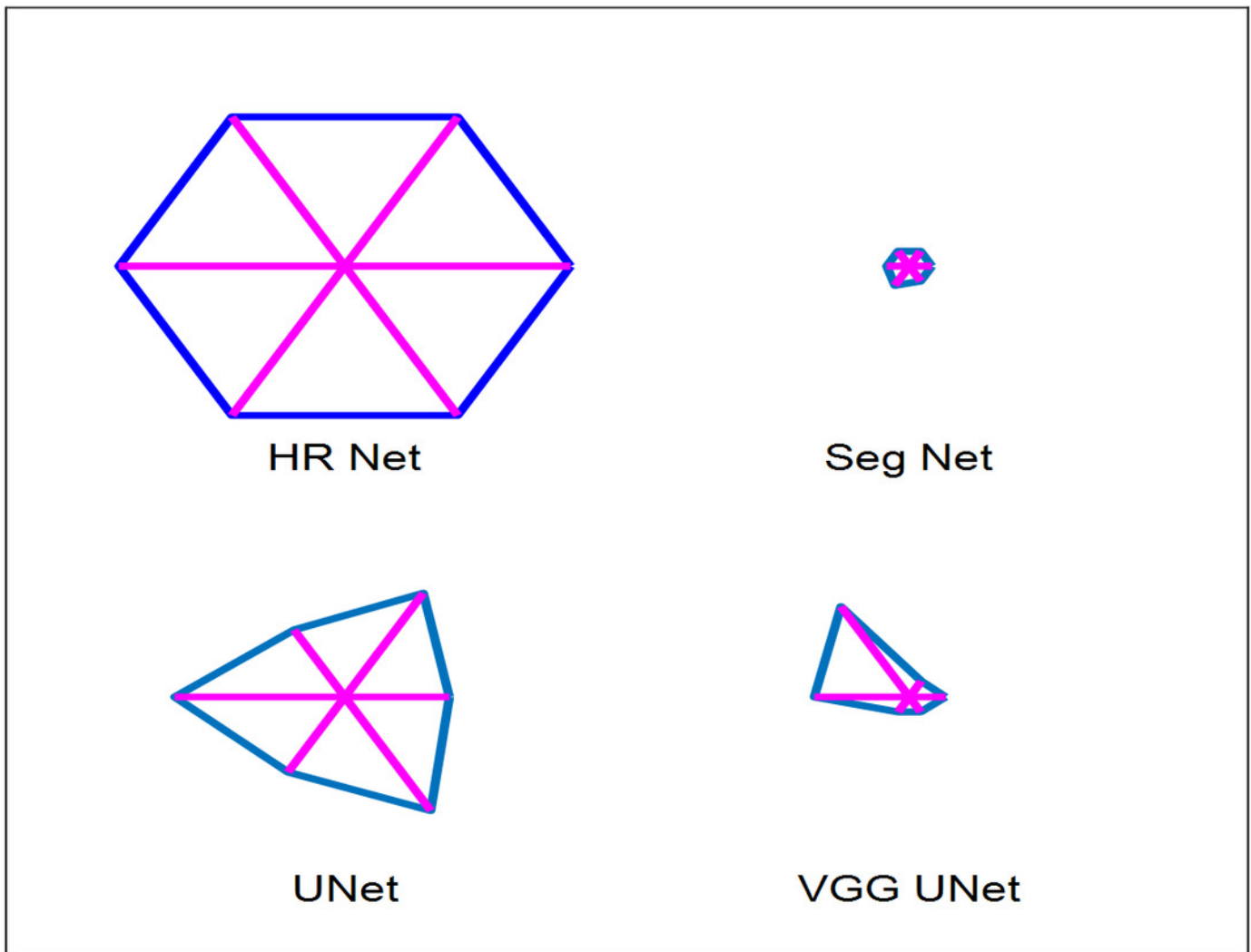


Table 1 (on next page)

Performance measures of segmentation performed on various models mentioned

1 Table 1. Performance measures of segmentation performed on various models mentioned

Method	TPrate= Sensitivity	TNrate= Specificity	Jaccard	Dice	Accuracy	Precision
HR_Net	0.8862	0.9930	0.8428	0.9147	0.9624	0.9593
Seg_Net	0.7859	0.7952	0.7962	0.8014	0.8816	0.8416
UNet	0.8215	0.9195	0.8143	0.8836	0.9105	0.9281
VGG_UNet	0.7918	0.7964	0.8224	0.8418	0.8794	0.8416

2

Table 2 (on next page)

Inference speed of the four models along with other parameters to affecting inference speed

- 1 Table 2: Inference speed of the four models along with other parameters to affecting inference
2 speed
3

Name of Model	Inference Time (ms)	Number of Layers	Number of Params	Model Size (MB)
UNet	42	32	7,759,521	30
SegNet	84	64	31,819,649	122
VGG UNet	65	85	25,882,433	99
HR Net	140	1043	28,607,456	112

4